Electronic Supplementary Information

A Butterfly−like Lead−doped Titanium−oxide Compound with High Performance in Photocatalytic Cycloaddition of CO_2 to Epoxide

Amir Said,[a] Guanyun Zhang,[a]* Caiyun Liu,[a] Dexin Wang,[a] Huihui Niu,[a] Yanshu Liu,[a] Guanjie Chen,[a] Chen—Ho Tung[a] and Yifeng Wang[ab]*

[a] *Key Lab for Colloid and Interface Science of Ministry of Education, School of Chemistry and Chemical Engineering, Shandong University, Jinan 250100, China*

[b] *State Key Laboratory of Crystal Materials, Shandong University, Jinan 250100, China*

*Email: guanyzhang@sdu.edu.cn, yifeng@sdu.edu.cn

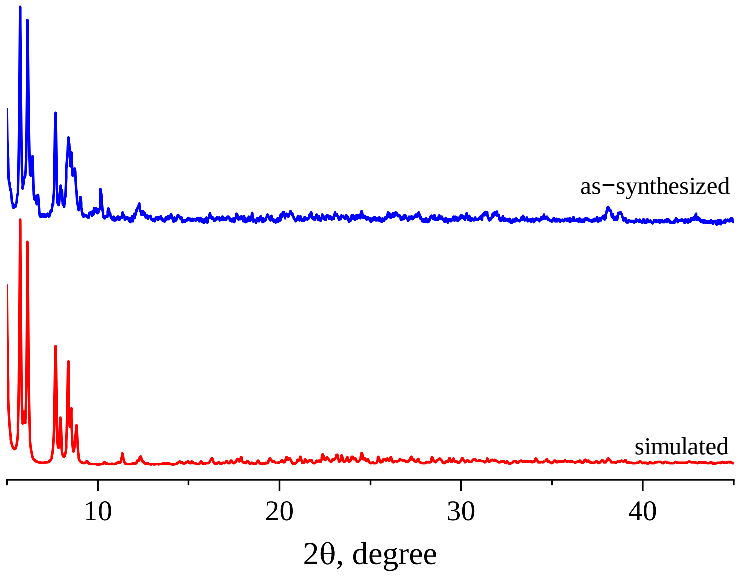

Fig. S1 The simulated and experimental PXRD pattern of **$Ti_{10}Pb_2$**. It can be seen from the profile that the experimentally obtained PXRD data are consistent with the simulated data obtained from the crystal structure.

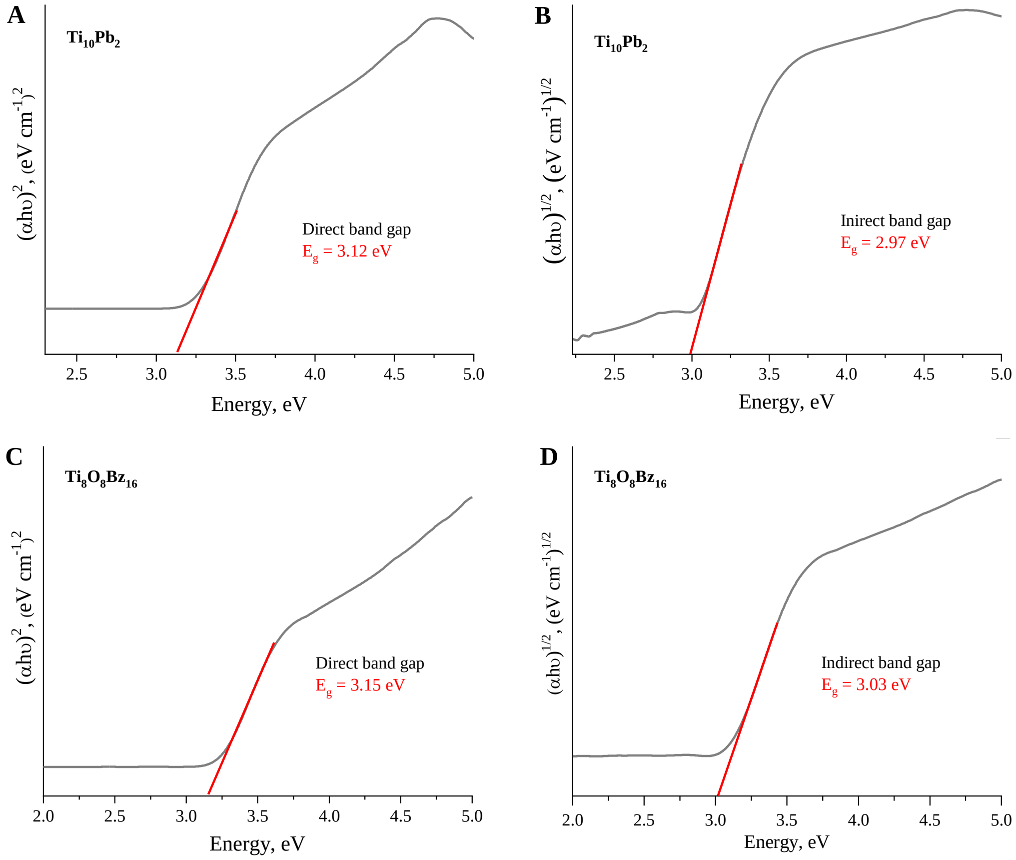

Fig. S2 Calculation of the band gap energies based on UV–vis diffuse reflectance spectra: (**A**) Direct band gap energy of **$Ti_{10}Pb_2$**, (**B**) indirect band gap energy of **$Ti_{10}Pb_2$**, (**C**) direct band gap energy of $Ti_8O_8Bz_{16}$ and (**D**) indirect band gap energy of $Ti_8O_8Bz_{16}$.

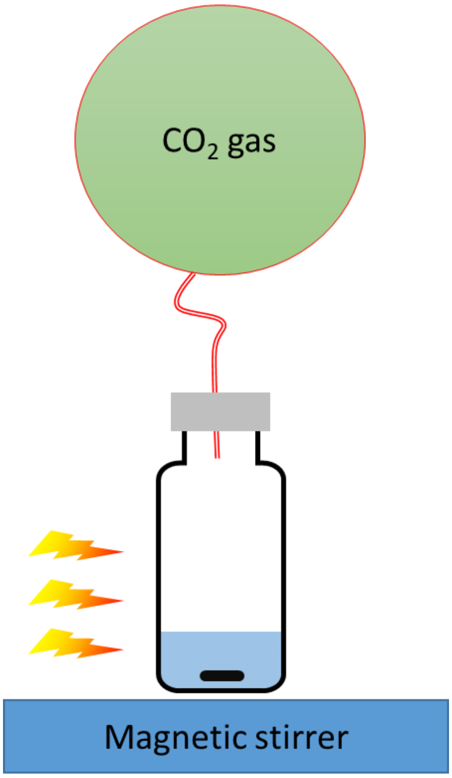

Fig. S3 An illustration of the experimental setup. Note that the balloon is not drawn to scale.

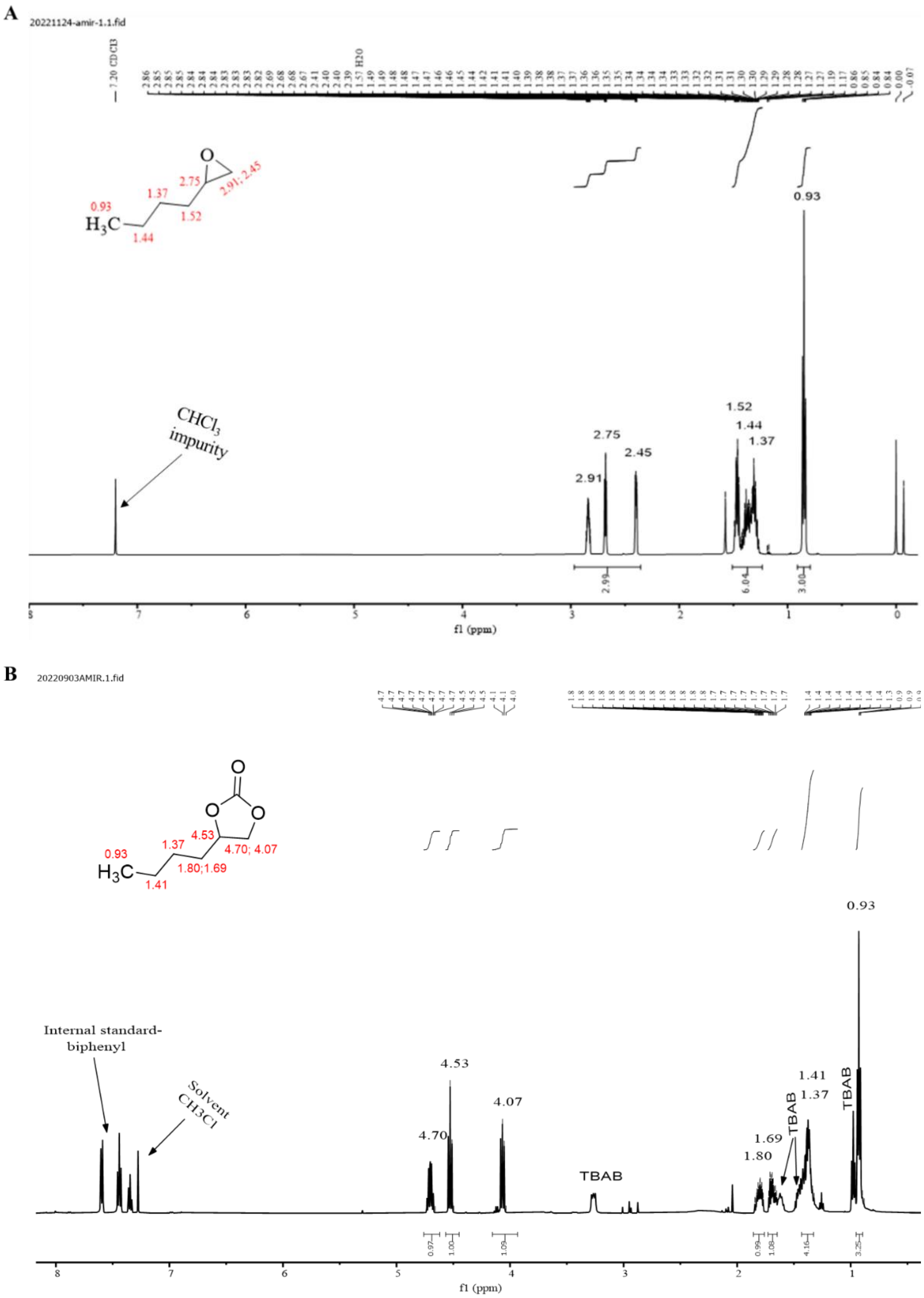

Fig. S4 ^{1}H NMR spectra before and after cycloaddition of CO_2 to epoxide.

Discussion: ^{1}H NMR was measured using a Bruker Avance−400 NMR spectrometer at room temperature using $CDCl_3$ as the solvent. The spectra show some peaks of 1,2−epoxyhexane at 2.45, 2.75 and 2.91 ppm before reaction (Fig. S4 A). After the catalytic reaction, these peaks diminished along with the production of new peaks of cyclic carbonate at 4.07, 4.53 and 4.7 ppm (Fig. S4 B). After 20 h of simulated solar light irradiation in 1 bar CO_2, the conversion of epoxide to cyclic carbonate approached completion.

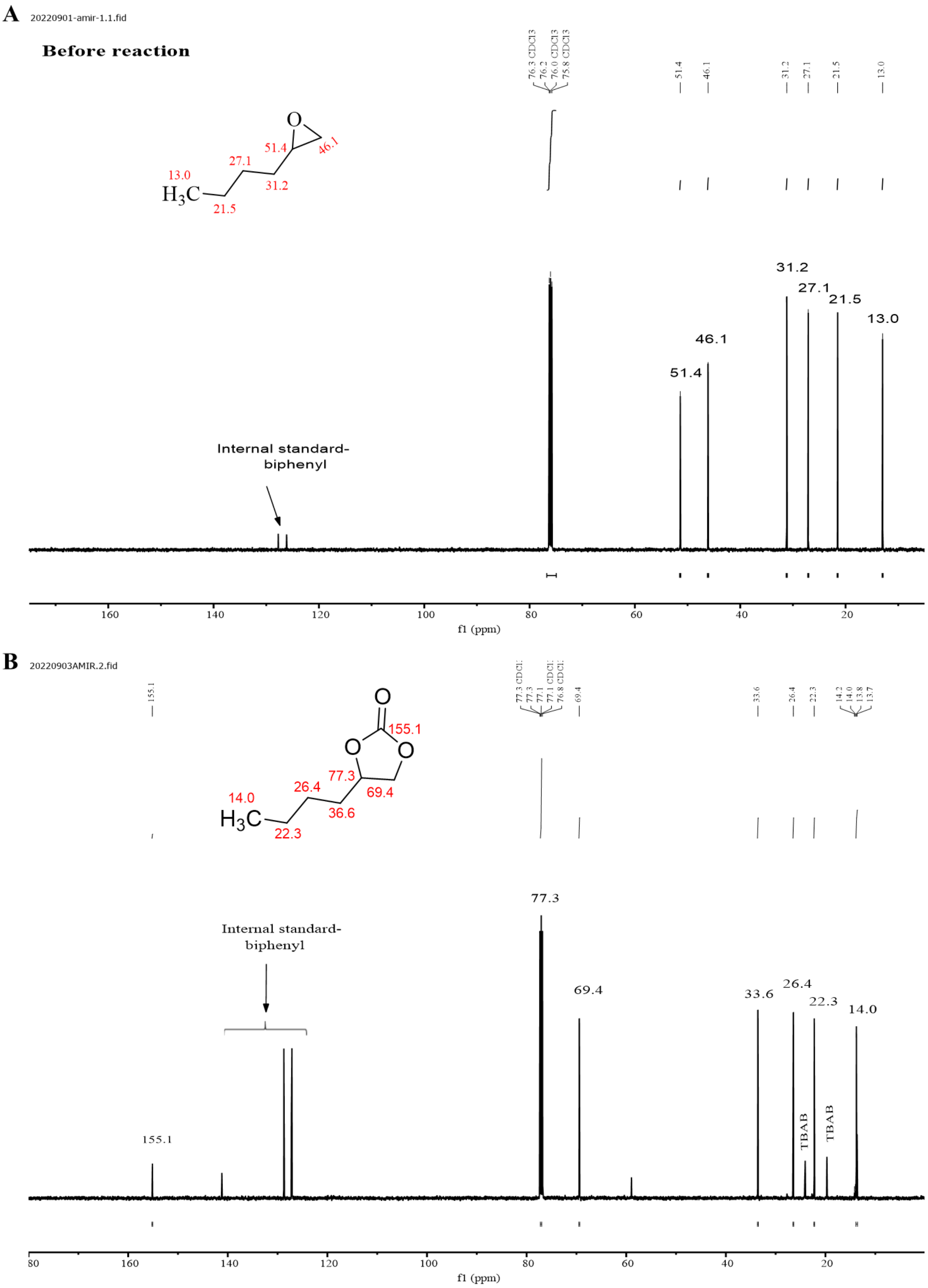

Fig. S5 ^{13}C NMR spectra before and after cycloaddition of CO_2 to epoxide.

Discussion: The ^{13}C NMR spectra show that there are some peaks of the 1,2−epoxyhexane at 46.1 and 51.4 ppm before the reaction (Fig. S5 A). After the reaction, these peaks diminished along with the production of new peaks of cyclic carbonate at 69.4, 77.3 and 155.1 ppm (Fig. S5 B).

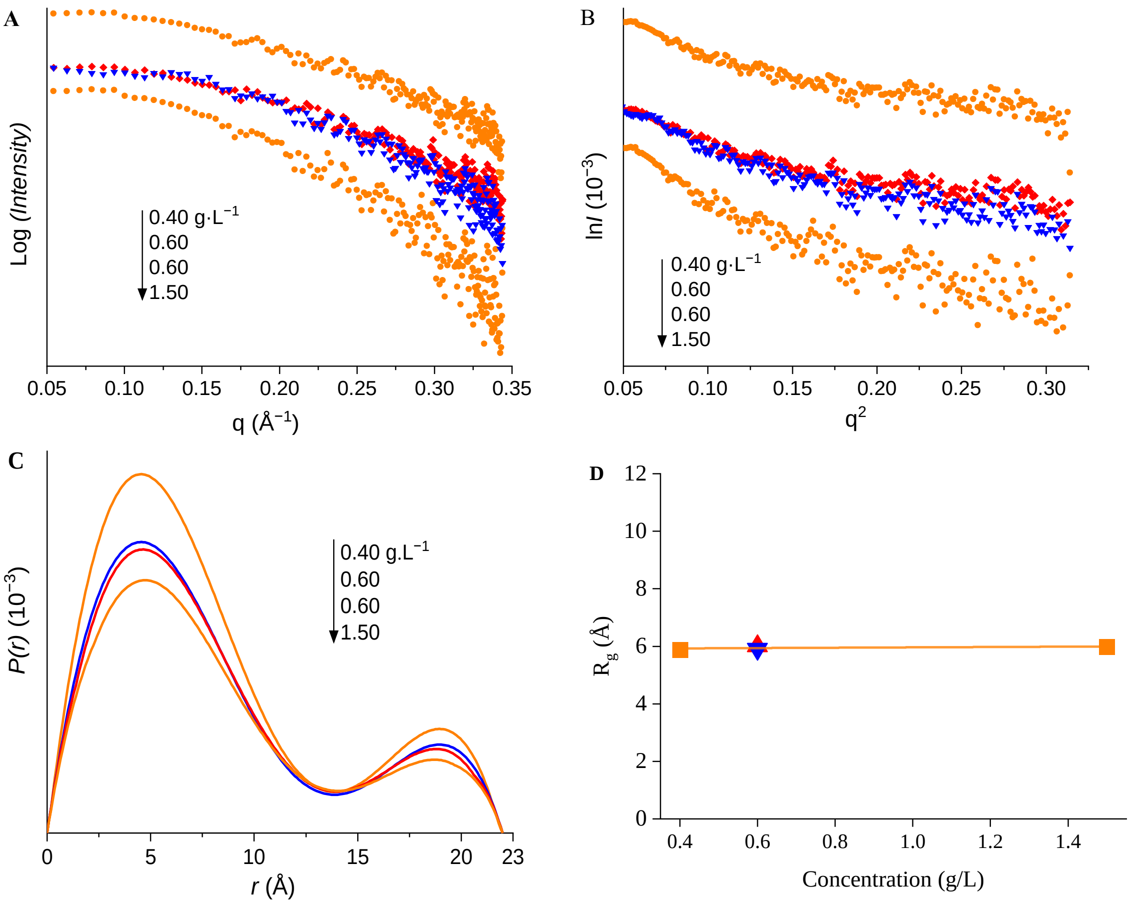

Fig. S6 Small–angle X–ray scattering patterns of **Ti$_{10}$Pb$_2$** in 1,2–epoxyhexane / dichloromethane (10%) solutions at various concentrations (orange) and those of the reaction solution before (red) and after (blue) the cycloaddition reaction of CO$_2$ with epoxide.

Discussion: After removing the background (a 1:9 v/v of epoxide/dichloromethane), the experimental results of SAXS analysis at different concentrations are shown in Fig. S6 A. Fig. S6 A has been changed to Fig. S6 B, in order to convey a better illustration between the ln$I$ and q^2 (low–Q region). After that, the SAXS Data Analysis software ATSAS 3.1.1 was used to figure out the key parameters, such as the zero–angle scattering intensity (I_0), pair distance distribution function (PDDF), and radius of gyration (R_g) (Fig. 6A and B in the text). These results show that the radius of gyration did not change with concentration when **Ti$_{10}$Pb$_2$** was dissolved in epoxide/dichloromethane (Fig. S6 D) and that the zero–angle scattering intensity is proportional to the concentration of **Ti$_{10}$Pb$_2$** in solution (inset of Fig. 6A in the text). The orange curves in Fig. S6 C represent P(r) of the **Ti$_{10}$Pb$_2$**/epoxide solution at various concentrations. These curves, as well as those of the solution samples before and after the reaction (red and blue), are entirely consistent with the simulation curve made using the crystal structure of **Ti$_{10}$Pb$_2$**. The SAXS study shows that **Ti$_{10}$Pb$_2$** is a genuine catalyst because its structure remained intact during the cycloaddition reaction of CO$_2$ with epoxide.

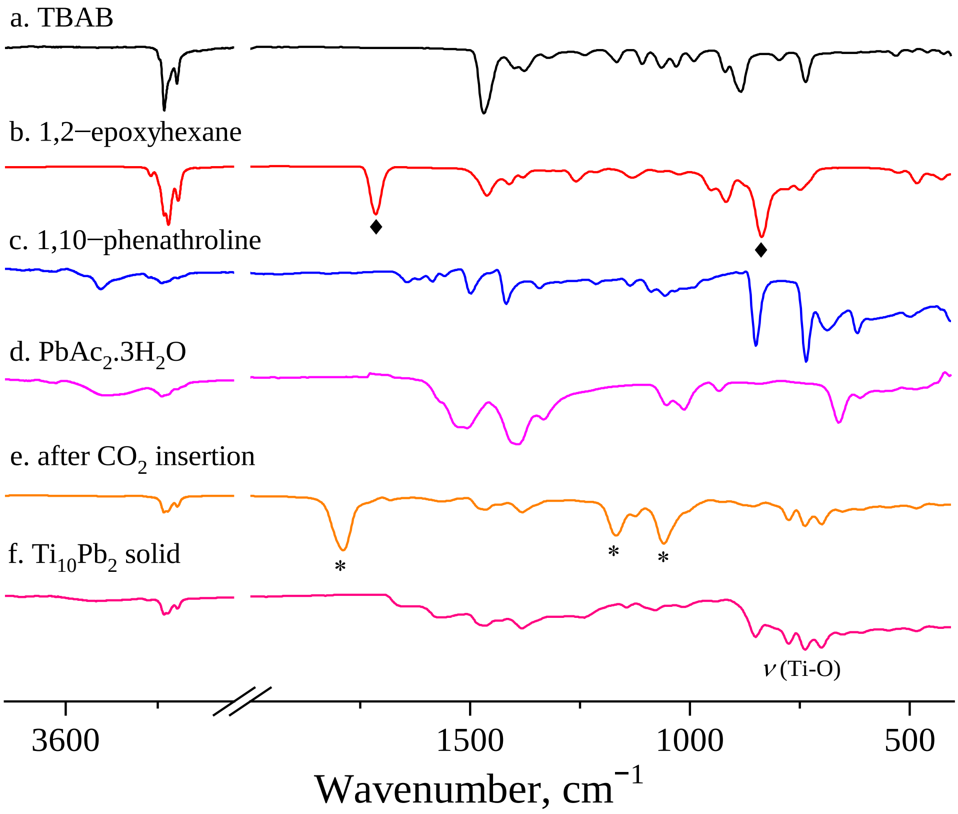

Fig. S7 FTIR spectra of various materials with **$Ti_{10}Pb_2$** before and after the CO_2 cycloaddition with 1,2−epoxyhexane.

Discussion: In the FTIR spectra, the peaks in curve b at 1715 and 836 cm^{-1} are assigned to 1,2−epoxyhexane (marked with ♦ in Fig. S7, curve b) and the peaks in curve f at 1789, 1169, and 1061 cm^{-1} are assigned as the cyclic carbonate product (marked with $*$ in Fig. S7, curve e). It can be seen that the epoxide peaks disappeared after the reaction completion. By comparing curves c and f, the peaks at 772 and 702 cm^{-1} are attributed to the stretching mode of Ti−O bonds of **$Ti_{10}Pb_2$**. By comparing curves e and f, the peak positions of Ti−O remained unchanged after the photocatalytic reaction, indicating that the structure of **$Ti_{10}Pb_2$** remained stable after the photocatalytic reaction and **$Ti_{10}Pb_2$** was the true photocatalyst.

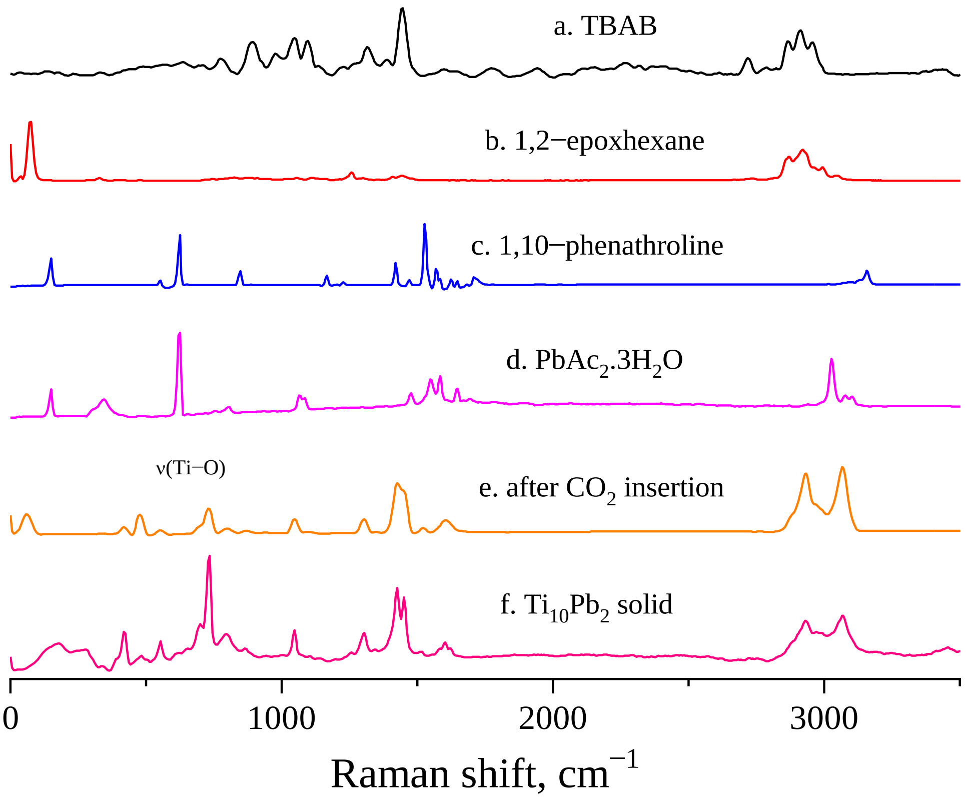

Fig. S8 Raman spectra of various materials with **Ti$_{10}$Pb$_2$** before and after the CO$_2$ cycloaddition with 1,2−epoxyhexane.

Discussion: In the Raman spectra, by comparing curves c and f (Fig. S8, in curve f), the peak at 731 cm^{-1} attributed to the stretching mode of Ti−O bonds, and the peaks at 1436 and 1595 cm^{-1} (in curve f) assigned the stretching modes of C−O and C−C bonds, respectively, of **Ti$_{10}$Pb$_2$**. The Raman peaks of the 1,2−epoxyhexane and cyclic carbonate products were not identified during the photocatalytic reaction. By comparing curves e and f (after the photocatalytic reaction and pure crystalline **Ti$_{10}$Pb$_2$**), the peak position of Ti−O remained unchanged, suggesting that the structure of **Ti$_{10}$Pb$_2$** remained intact after the photocatalytic reaction and **Ti$_{10}$Pb$_2$** was the genuine photocatalyst.

Table S1. Comparison of **Ti$_{10}$Pb$_2$** with the various catalysts which were used for the cycloaddition of CO$_2$ to epoxide.

Catalyst type	**Temp., °C**	**Reaction time, h**	**CO$_2$ Pressure, bar**	**Conv. %**	**Yield, %**	**References**
Ti$_{10}$Pb$_2$	80	2	1	>99	>99	*This study*
Ti$_{10}$Pb$_2$	20	20	1	>99	>99	*This study*
Co(II)Mg(II)	140	6	1	>99	>99	*Nat. Chem.*, 2020, **12**, 372–80.
g–C$_3$N$_4$–S	130	4	35	>99	96.7	*Catal. Sci. Technol.*, 2016, **6**, 2942–2948.
BiNbO$_4$/5%r–GO	70	11	1.4	–	65	*Chem. Eng.,* 2020, **24**, 12072–12079.
I–Co$_3$O$_4$	80	5	1	72	47.4	*Ind. Eng. Chem. Res.,* 2021, **60**, 15106–15114.
PMo$_{12}$@Zr–Fc MOF	80	8	1	–	86.77	*Appl. Catal. B Environ.,* 2021, **296**, 120329.
CoPc/TiO$_2$	25	24	1	96.7	94	*ACS Sustainable Chem. Eng.*, 2018*,* **6**, 15653–15661.
MTS–1(3)–AT–2	120	6	16	98.3	82.2	*ACS Appl. Mater. Interfaces*, 2018, **10**, 22119–22129.
chiral (salen)CrCl$_3$ complex	80 °C	24	52	–	>99	*J. Am. Chem. Soc.,* 2002, **124**, 6335–6342.
Al–complexes 2a.	120	1	30	–	74.3	*ACS Catal.,* 2012, **2**, 2029–2035.
HPC–800	r.t.	10	1	–	95	*Angew. Chem. Int. Ed.,* 2019, **58**, 3511.
Zr–MOF	r.t.	6	1	–	>99	*ACS Catal.,* 2021, ***11***, 1988.
PMo$_{12}$@Zr–Fc MOF	80	8	1	–	85	*Appl. Catal. B Environ.,* 2021, **296**, 120329.
Ni–TCPE	100	12	10	–	>99	*J. Am. Chem. Soc.,* 2015, **137**, 15066–15069.
Zn–Asp–300	r.t.	4	1	96.3	92.0	*Appl. Surf. Sci.,* 2021, **540** 148311.
Co(III)/M(I)	70	4	30	–	>99	*J. Am. Chem. Soc.,* 2020, **142**, 19150–19160.
[Zn$_2$(TCA)(BIB)$_{2.5}$]·(NO$_3$)	60	1	1	–	>99	*Inorg. Chem.,* 2018, **57**, 11157–11164.
[PPN]Cl	100	12	20	–	98	*J. Am. Chem. Soc.,* 2011, **133**, 10720–10723.
Au$_{19}$Ag$_4$	60	24	20	–	80	*Angew. Chem. Int. Ed.,* 2021, **60**, 10573.
MOF–801	80	15	1	99	92	*J. Mater. Chem. A,* 2022, **10**, 10051–10061
Cat1–cat8	25	48	4	99	99	*ACS Appl. Mater. Interfaces*, 2021, **13**, 8344–8352
(COP)–222	100	24	1	99	99	*Chem.*, 2019, **5**, 3232–3242
MOFs 1	80	18	1	99	99	*Chem. Eur. J.* 2018, **24**, 15831–15839
ZnMOF–1	40	4.5	1	99	99	*ChemCatChem* 2018, **10**, 2401–2408
Zn–DABCO	100	12	8	–	100	ChemistryOpen, 2017, **6**, 674–680
CoMOF–2	40	8	1	99	99	*Inorg. Chem.,* 2019, **58**, 10084–10096
CoMOF–10	60	24	1	99	99	*J. Mater. Chem. A*, 2019, **7**, 2884–2894
ZnMOF–1	40	4.5	1	99	99	*ChemCatChem*, 2018, **10**, 2401–2408